

# Image Cover Sheet

**CLASSIFICATION**

**SYSTEM NUMBER**

38697

UNCLASSIFIED



**TITLE**

THE STUDY OF PROPELLER CAVITATION NOISE USING CROSS-CORRELATION METHODS

**System Number:**

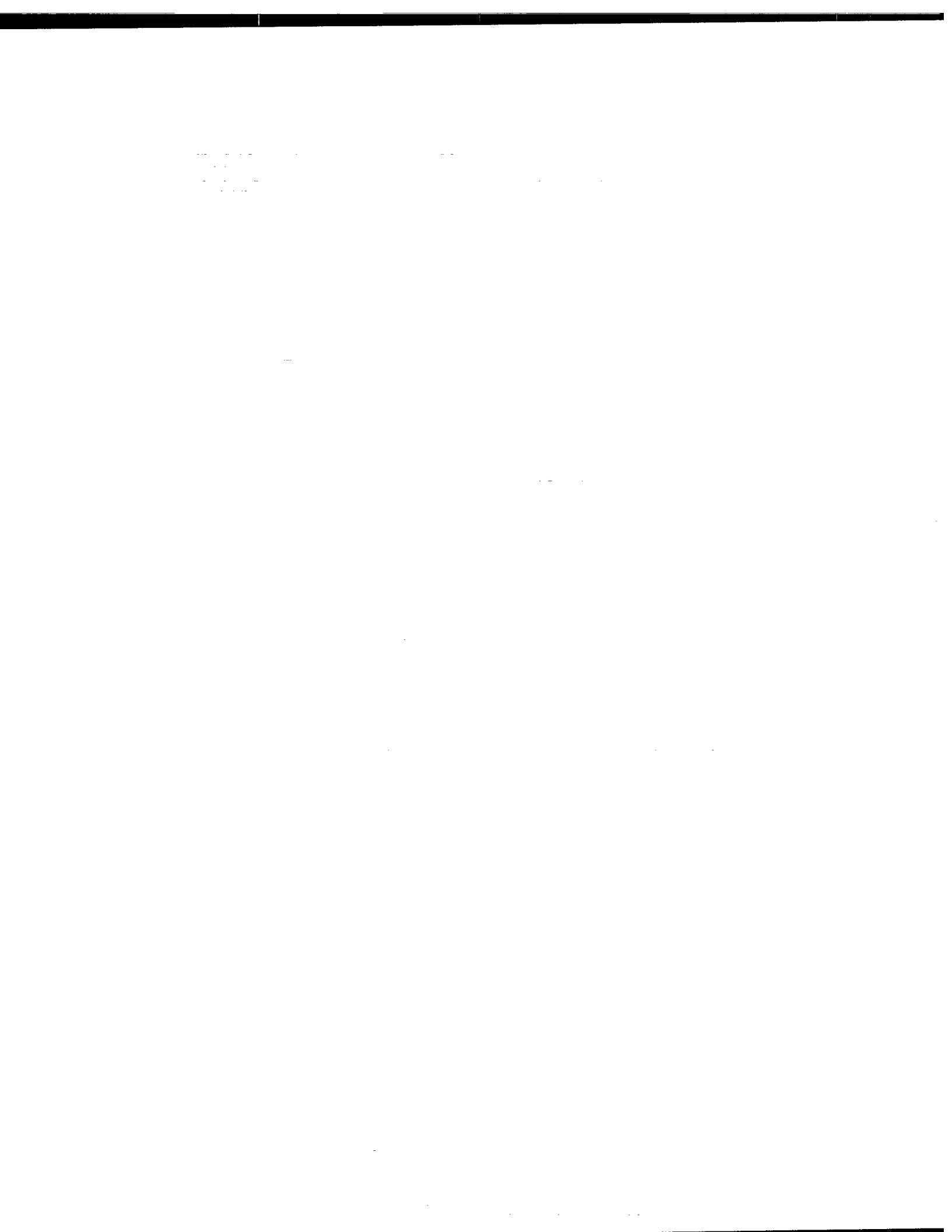
**Patron Number:**

**Requester:**

**Notes:**

**DSIS Use only:**

**Deliver to:** JR



DEFENCE RESEARCH ESTABLISHMENT  
ATLANTIC

DARTMOUTH N.S.

D. R. E. A. REPORT 82 / 5

THE STUDY OF PROPELLER CAVITATION NOISE  
USING CROSS-CORRELATION METHODS

L. J. Leggat and N. C. Sponagle

December 1982

Approved by T. Garrett

Director / Technology Division

DISTRIBUTION APPROVED BY



CHIEF D. R. E. A.

RESEARCH AND DEVELOPMENT BRANCH  
DEPARTMENT OF NATIONAL DEFENCE  
CANADA

## RESUME

Ce rapport présente une méthode permettant d'étudier les mécanismes responsables de la production de bruit par les hélices cavitantes. La méthode expérimentale est basée sur l'établissement de corrélations croisées entre le gradient de pression dans le champ rapproché de l'hélice et la bruit dans le champ éloigné de cette dernière et permet de déterminer la répartition spatiale de la puissance de la source acoustique sur l'hélice cavitante et à proximité de celle-ci.

On présente les fondements mathématiques de la méthode des corrélations croisées puis certains des résultats d'expériences effectuées à l'aide d'hélices spécifiquement conçues pour la production de cavitation sous forme de vortex et de bulles.

Les corrélations croisées établies pour un certain nombre de points le long d'une trajectoire parallèle à l'axe de l'hélice indiquent que la plus grande partie du bruit émis par des hélices produisant une cavitation sous forme de vortex provient de la zone d'effondrement des vortex. Dans le cas d'une hélice engendrant une cavitation sous forme de bulles on constate une répartition relativement constante de la puissance de la source de la région du disque de l'hélice vers l'aval jusqu'au point d'effondrement des vortex. Toutes les hélices mises à l'épreuve présentaient un lent affaiblissement de la puissance de la source acoustique en fonction de la distance vers l'aval derrière l'effondrement des vortex. Ces résultats peuvent constituer un indice du fait qu'une part importante du bruit est produite par le rebondissement des bulles dans le sillage de l'hélice.

## THE STUDY OF PROPELLER CAVITATION NOISE USING CROSS-CORRELATION METHODS

L. J. Leggat and N. C. Sponagle  
Defence Research Establishment Atlantic  
Dartmouth, Nova Scotia, Canada

### ABSTRACT

This paper presents a technique for the study of the mechanisms responsible for the generation of noise from cavitating propellers. The experimental method, which involves the cross-correlation of the pressure gradient in the near-field of the propeller with the far-field sound, allows the determination of the spatial distribution of acoustic source strength on and near the cavitating propeller.

The paper describes the mathematical basis for the cross-correlation technique, and then presents some of the results from experiments with propellers specifically designed to produce vortex and bubble forms of cavitation.

Cross-correlations performed at a number of points along a track parallel to the axis of the propeller indicate that most of the

noise from propellers producing vortex cavitation originates from the region of vortex collapse. A bubble cavitation propeller showed a region of relatively constant source strength distribution from the propeller disk region downstream to the point of vortex collapse. All propellers tested showed a slow decay of acoustic source strength with downstream distance after vortex collapse. This result may be indicative of significant amounts of sound being produced by bubble rebounds in the propeller wake.

### INTRODUCTION

In recent years, the noise produced by hydrodynamic flow past rigid or flexible surfaces has been the subject of considerable interest. It is known that in non-cavitating fluid flows the noise is produced by a variety of mechanisms, most notably fluctuating forces caused by variations in

### NOTATION

$a_0$	speed of sound
$a_1, a_2$	amplitudes
$B$	bandwidth
$f_i, \underline{f}$	local surface stress tensor, vector
$f_0$	centre frequency
$p$	far-field acoustic pressure or local pressure
$\nabla p_n$	normal pressure gradient
$\underline{r}$	distance between source and far-field measuring point
$R_{xy}(\tau)$	cross-correlation between variables $x$ and $y$
$S$	surface
$T_{ij}$	effective stress tensor
$t$	time
$\hat{t}$	retarded time $t = \hat{t} - x/a_0$
$u$	velocity
$u_i, u_j$	velocity vectors

$u_n$	normal velocity
$V$	volume
$X$	Dimensionless propeller radius
$\underline{x}$	$\underline{x} = (x-y)$ distance from source point to far-field microphone
$x_i, \underline{x}$	space co-ordinate to indicate point of sound detection in the far-field
$y_i, \underline{y}$	space co-ordinate used in source region
$\delta_{ij}$	Kronecker delta tensor
$\lambda$	wavelength of sound
$\rho$	ambient density
$\rho'$	density fluctuation
$\tau$	retarded time delay between two realizations of fluctuating variables
$\tau_{ij}$	viscous stress tensor
.	a dot over a symbol indicates derivatives with respect to time

the magnitude and incidence of the inflow velocity. Other mechanisms such as incident turbulence, turbulent boundary layers, separated flows and vortex shedding may be important in non-cavitating flows. These mechanisms can all be described as dipoles whose acoustic efficiencies are dependent upon the square of the Mach number.

In flows where cavitation occurs, these dipole mechanisms are of secondary importance to the growth and collapse of cavitation cavities. Cavitation behaves as a monopole mechanism whose acoustic efficiency is dependent upon the Mach number. In circumstances where the Mach number is small such as for the flow past a marine propeller, the monopole and dipole acoustic efficiencies are such that cavitation is the predominant source of noise.

Cavitation on a marine propeller can appear in a number of forms. Three of the more common types are vortex, sheet, and bubble cavitation. Vortex cavitation is generated in the low pressure regions of the hub and tip vortices. Sheet and bubble cavitation can occur on both the face and the back of a propeller blade. The back, however, is more likely to experience these forms of cavitation owing to the low pressure on this side of the blade. The occurrence and the extent of these forms of cavitation are dependent upon the propeller design, the operating condition of the propeller, and the flow in which the propeller operates. During conditions of moderate to high propeller loading, it is not unusual to find two or more types of cavitation simultaneously present on the propeller.

In reduced-noise propeller design, attempts are made to avoid the noisier types of cavitation, and special design practices are adopted to control the noise produced by the remaining types. However, the effectiveness of the noise control is very much dependent upon the designers' notion of the mechanism responsible for the noise generation. While it is generally agreed that cavitation noise is produced by the growth, collapse and rebounding of vapour bubbles, the issue becomes obscure when considering the more intricate sheet and vortex cavitation types. More precise knowledge of the mechanisms responsible for the noise and the distribution of sources on and near the blade should assist present effort in the field of propeller noise reduction.

The study of propeller radiated noise due to cavitation on the propeller is presently carried out using two methods. The first, propeller viewing and sound ranging, is carried out on full scale ships. The propellers are viewed through ports in the bottom of the ship's hull, above the propeller. Ideally, sound ranging is carried out simultaneously. It

is a fairly simple procedure to determine the spectral content of the first type of cavitation to occur on the blade. Generally, tip vortex cavitation appears first. However, if more than one form occurs, it is impossible to discriminate the contribution to the far-field signal from the various forms of cavitation on the blade.

The second method used to study propeller cavitation and radiated noise is through model testing in cavitation tunnels and towing tanks. This procedure suffers from the same deficiencies as the full scale experiments; however, it has the added complication that the sound measurements have to be made inside the tunnel or tank. The resulting sound data represents the near field propeller pressure field in a highly reverberant space. It is therefore difficult to obtain meaningful acoustic data over a wide frequency range and to discriminate between the source strengths of the different forms of cavitation.

The present paper describes an experimental method for obtaining the acoustic source strengths of various forms of propeller cavitation and the results obtained from some tests with cavitating propellers. The method, based on Curle's formulation of flow noise theory<sup>1</sup>, makes use of the cross-correlation between the normal pressure gradient in the near-field of the cavitation and the acoustic pressure in far-field. The technique is an extension of established methods for determining the acoustic source strength in aerodynamic flows about solid surfaces, in air jets, and on the surfaces of fan blades.<sup>2,3,4,5</sup> The method discriminates in favour of that part of the near-field pressure gradient fluctuation which contributes to the far-field acoustic pressure. Because the normal pressure gradient is directly proportional to the cavity normal velocity through Euler's equation, a direct evaluation of the local acoustic source strength, intensity, spectrum, and correlation area is possible. In this way the different forms of propeller cavitation can be studied independently leading to improved concepts of the physical mechanisms responsible for the noise, and to more accurate scaling laws and prediction techniques. The propeller designer, knowing the relative acoustic intensity and cause of each form of cavitation, will be better prepared to produce a design which discriminates against the noisier forms of hydrodynamic cavitation.

## THEORETICAL DEVELOPMENT

### Application of Curle's General Aerodynamic Noise Equation

The acoustic radiation from a region of unsteady flow containing a surface is given by Curle's generalized solution to the Lighthill Equation<sup>6</sup>, (see Figure 1),

$$\begin{aligned}
 a_0^2 \rho'(\underline{x}, t) = & \int_S \left[ \frac{\delta}{\delta t} (\rho u_n) \right] \frac{dS}{4\pi x} \\
 & - \frac{\delta}{\delta x_i} \int_S \left[ f_i + \rho u_i u_n \right] \frac{dS}{4\pi x} \\
 & - \frac{\delta^2}{\delta x_i \delta x_j} \int_V \left[ \frac{T_{ij}}{4\pi x} \right] dV
 \end{aligned} \quad (1)$$

where  $\rho'$  is the incremental density disturbance relative to the ambient density  $\rho$ , and  $a_0$  is the ambient speed of sound. The square brackets denote evaluation at retarded time  $\hat{t} = t - x/a_0$ . The first two integrals are associated with noise generated by the flow passing over the surface  $S$ , which may deform with a velocity  $u_n$ . The quantity  $f_i$  represents the local stress acting at each point on the surface. The vector  $\underline{f}$  may comprise both shear stress and normal stress components. The third integral is the Lighthill volume integral for turbulence-generated quadrupole noise where  $T_{ij}$ , the effective stress tensor, is given by

$$T_{ij} = \rho u_i u_j + \tau_{ij} + (p - a_0^2 \rho') \delta_{ij} \quad (2)$$

where  $\rho u_i u_j$  is the Reynolds stress,  $\tau_{ij}$ , the viscous stress and  $(p - a_0^2 \rho') \delta_{ij}$  the thermal stress.

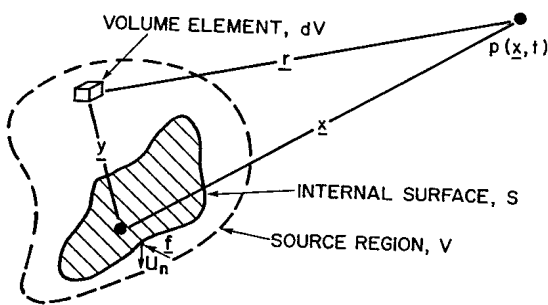


Fig. 1. Terminology for Generalized Noise source

In the geometric and acoustic far-field, where  $r^2 \gg S$ , and  $r \gg \lambda$ , the spatial derivatives can be shown to become time derivatives and  $r = (\underline{x} - \underline{y}) \approx x$  such that

$$\begin{aligned}
 p(\underline{x}, t) \approx & \frac{1}{4\pi x} \int_S \left[ \rho \dot{u}_n \right] dS \\
 & + \frac{x_i}{4\pi x^2 a_0} \int_S \left[ \frac{\delta}{\delta t} (f_i + \rho u_i u_n) \right] dS \\
 & + \frac{x_i x_j}{4\pi x^3 a_0} \int_V \left[ \frac{\delta^2}{\delta t^2} \frac{T_{ij}}{4\pi x} \right] dV
 \end{aligned} \quad (3)$$

For hydrodynamic flow noise, the quadrupole noise is minimal, and so attention is directed to the two surface integrals. For cases where cavitation occurs on the blades and at low Mach numbers, the contributions from the second integral are small giving

$$p(\underline{x}, t) \approx \frac{1}{4\pi x} \int_S \left[ \rho \dot{u}_n \right] dS \quad (4)$$

This equation gives the acoustic pressure produced by a monopole with surface velocity  $u_n$ . For a propeller, acoustic radiation results from monopoles on and near the surface of the blade associated with the growth and collapse of cavitation. Because the surface velocity of the cavitation is difficult to measure, we substitute the normal pressure gradient by use of Euler's equation of linear momentum,

$$\frac{\delta}{\delta t} u_n = -\frac{1}{\rho} \nabla p_n \quad (5)$$

where  $\nabla p_n$  is the normal pressure gradient. Substituting equation (5) into equation (4) we obtain

$$p(\underline{x}, t) \approx -\frac{1}{4\pi x} \int_S \left[ \nabla p_n \right] dS \quad (6)$$

### The Causality Formalism

If both sides of equation (6) are multiplied by the far-field radiated pressure at a new time,  $t'$ , time averaging yields

$$\overline{p(t)p(t')} \approx -\frac{1}{4\pi x} \int_S \left[ \overline{\nabla p_n(\underline{y}, \hat{t}) p(\underline{x}, t')} \right] dS \quad (7)$$

If  $p$  and  $\nabla p_n$  are stationary random variables,

$$\overline{pp(\underline{x}, \tau)} \approx -\frac{1}{4\pi x} \int_S \left[ \overline{\nabla p_n p} \right]_{\tau + x/a_0} dS \quad (8)$$

where  $\tau = t - t'$

The expression for the mean square acoustic pressure is given when  $\tau = 0$ . Thus,

$$\overline{p^2}(\underline{x}) \approx -\frac{1}{4\pi x} \int_S \left[ \overline{\nabla p_n p} \right] dS \quad (9)$$

$x/a_0$

and,

$$\frac{d\overline{p^2}}{dS} \approx -\frac{1}{4\pi x} \left[ \overline{\nabla p_n p} \right] \quad (10)$$

$x/a_0$

Thus the contribution to the mean square sound pressure at a far field point  $\underline{x}$  arriving from an element above the blade surface  $dS(\underline{y})$  where  $\nabla p_n$  is being measured is given by the integrand of equation (9). The quantity  $d\overline{p^2}/dS$  (Equation (10)) may be viewed as the strength of the acoustic source at a near-field point, and for the case where the monopole sound radiation is dominant, it will be called the surface monopole source strength.

Typically, the cross-correlation function will be similar to that shown in Figure 2. The amplitude of the correlation function is evaluated at the appropriate time delay, thus yielding a source strength associated with the monopole strength in the region of the measurement.

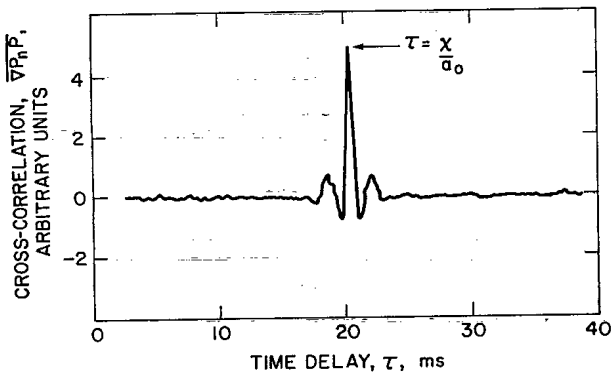


Figure 2. Cross-Correlation Function

The magnitude and phase of the source region's pressure intensity spectrum may be evaluated simply by performing the Fourier transform of the cross-correlation function in the vicinity of the appropriate time delay  $x/a_0$ . By performing many cross-correlations between the near-field pressure gradient and far-field sound at various points near the propeller and in its wake, it is possible to determine the distribution of acoustic source strength produced by a cavitating propeller.

#### EXPERIMENTAL METHOD

##### Apparatus

A complete description of the Defence Research Establishment Atlantic (DREA) propeller noise facility and its

capabilities is given in Reference 7. A shortened version is presented here.

The experiments are carried out in the well of the DREA Acoustic Barge<sup>8</sup>, located in Bedford Basin. The Basin has a mean depth of 50 m and the bottom is covered with a deep layer of silt, giving it good acoustic absorption properties.

Model propellers designed to produce various forms of cavitation are driven by a stationary drive pod suspended 2.67 m below the water surface as shown in Figure 3. The 26.5 kW electric motor installed in the pod will drive a 250 mm diameter propeller at revolution rates in excess of 2000 rpm. Instrumentation installed in the pod allows the measurement of propeller revolution rate and torque.

The propeller cavitation state is observed or photographed through a periscope fitted to one of the barge well cross-trollies. Lighting is provided by two high intensity strobe lamps mounted in water tight containers and fixed to a frame above the drive pod.

A pressure gradient hydrophone was designed and built at DREA to enable measurement of the  $\nabla p_n p$  term of Equation (10)<sup>9</sup>. This hydrophone, shown in Figure 4, consists of two ceramic cylinders mounted to a cylindrical probe. The two elements are gain and phase matched. The pressure difference,  $\Delta p/\Delta x$ , an approximation of the pressure gradient, is measured by differencing the signals from the two elements. The spacing between the two elements (31.8 mm) makes the hydrophone effective over the frequency range of 1 to 20 kHz.

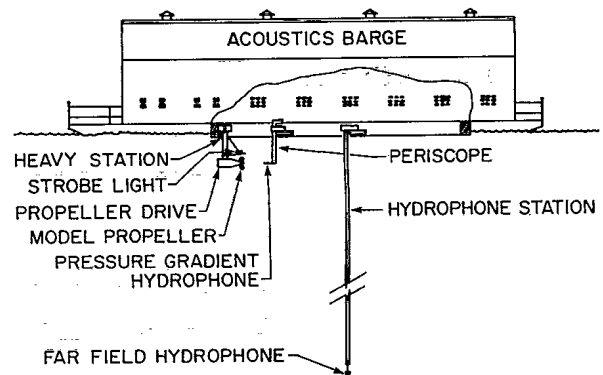


Figure 3. Propeller Drive and Hydrophone Layout

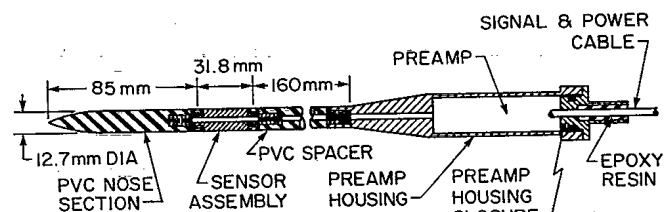


Figure 4. Pressure Gradient Hydrophone



The hydrophone was calibrated using the substitution technique. The sensitivity of the hydrophone is  $-200$  dB re  $1 \text{ V}/\mu\text{Pa}$  at  $1.0$  kHz, and increases at  $6$  dB per octave to  $20.0$  kHz, where the response deteriorates as a result of the half wavelength of the sound approaching the ceramic crystal spacing. The directivity of the hydrophone is the expected cosine pattern with broad-side rejection varying from  $10$  dB at  $1.0$  kHz to  $32$  dB at  $10.0$  kHz.

### Propellers

Three propellers were designed for the initial experiments. They are two-bladed fixed-pitch propellers,  $250$  mm in diameter, and were designed especially for the bollard pull condition. Experiments were carried out with the three propellers, which are shown in Figure 5 along with their associated cavitation patterns. One was designed to produce extreme tip vortex cavitation, a second to produce normal tip vortex cavitation simultaneously with hub vortex cavitation, and a third to produce bubble cavitation. These will be referred to as the Tip Vortex No. 1 propeller, Tip Vortex No. 2 propeller and Back Bubble propeller, respectively.

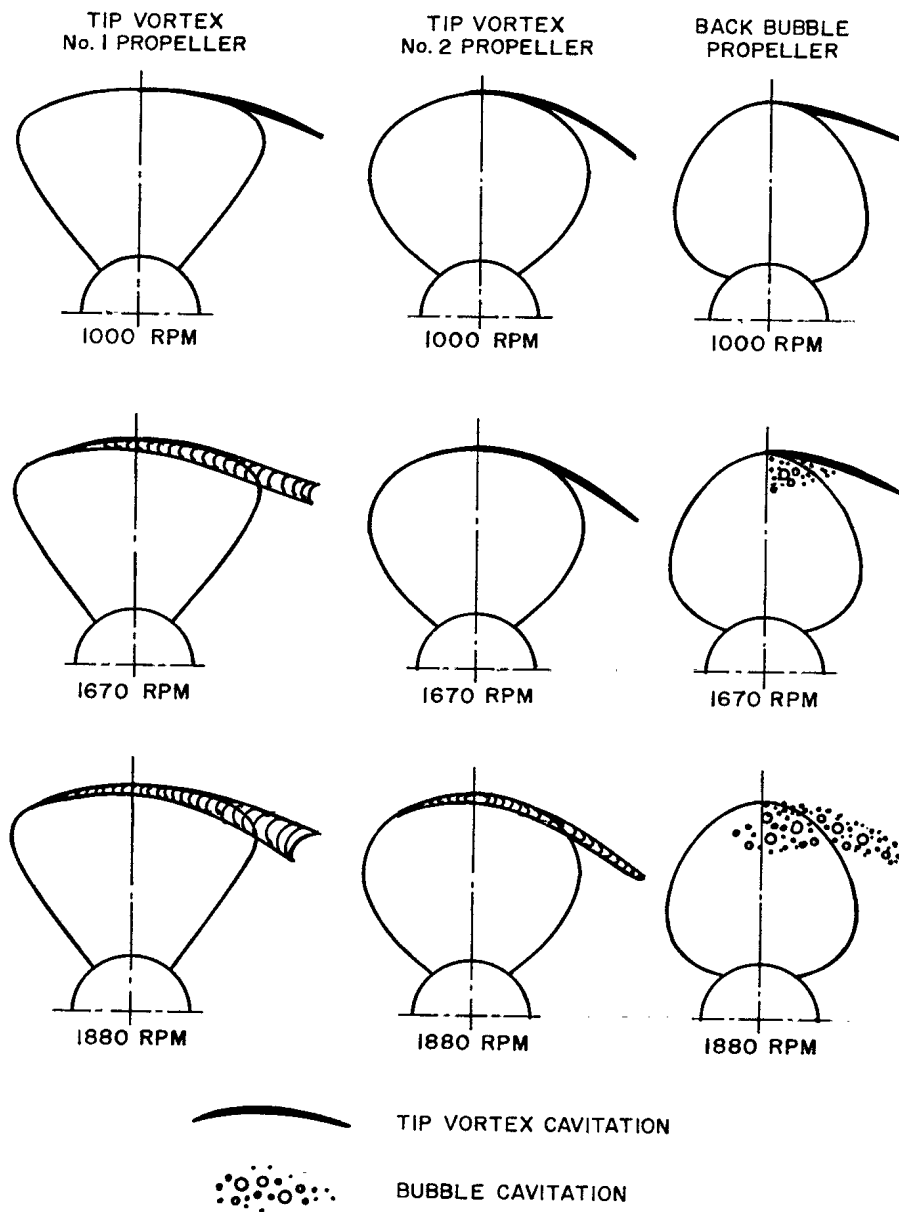


Figure 5.

Cavitation Patterns for the Three Research Propellers

The Tip Vortex No. 2 propeller and the Back bubble propeller were designed with a spanwise circulation distribution that would normally be associated with reduced noise propellers, while the Tip Vortex No. 1 propeller has a circulation distribution biased toward the tip as shown in Figure 6. The two tip vortex propellers were designed so that bubble and sheet types of cavitation would be avoided, and only vortex types of cavitation would be present. The Back Bubble propeller was given excessive camber to encourage the development of bubble cavitation.

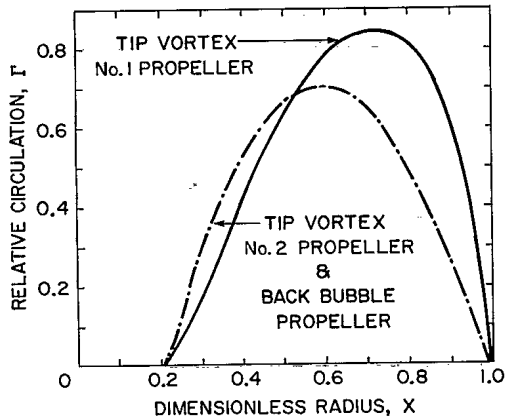


Figure 6. Propeller Circulation Distribution

Some Geometry Considerations

The theory developed earlier, which allows the determination of acoustic source strength distribution near the propeller depends upon being able to evaluate the magnitude of the cross-correlation function  $\overline{v_{pp}}$  at the correct time delay. The typical cross-correlation function shown in Figure 2 is representative of one obtained in an anechoic environment. The time delay of the peak corresponds to the time required for the sound to travel from the near-field pressure gradient hydrophone to the far-field hydrophone.

With the experimental arrangement shown in Figure 3, reflections of the sound from the propeller occur at the water surface and at the barge well side walls. The time taken for the sound travelling by these reflective paths to arrive at the far-field measuring point is greater than that for the direct path. As a result, additional peaks occur in the correlation function. When the arrival time of the direct path is close to that of the reflected paths, overlap of the peaks can occur. This generally results in errors being introduced into the direct path information. Also, as the bandwidth of the source signal decreases, the correlation function becomes more like a damped periodic function. The limit of zero bandwidth corresponds to a sine wave, the correlation of which is a cosine wave. For these cases where the source signal contains significant

amounts of periodic information, it is virtually impossible to differentiate between the direct and reflected paths of the correlation function. Thus to obtain meaningful results from this technique in a non-anechoic environment, the geometry of the source and hydrophones must be selected so that the error from the reflective contribution to the correlation function is minimized.

Before commencing experiments with model propellers, an analysis of this problem was carried out. Experiments were conducted using a J-11 projector as a source driven by a white noise generator. Through filtering, the bandwidth of the source signal was varied for various source to receiver spacings. This allowed an investigation of the effect on the correlation function overlap of both source bandwidth and source to receiver spacing.

A typical result showing the effect of bandwidth on the correlation function is shown in Figure 7. The top trace, which shows a correlation function with adequate time difference between the direct and reflected paths, allows a confident evaluation of the magnitude of the correlation function corresponding to the direct path. Note in this trace that the surface reflection appears as a negative-going peak owing to the pressure-release surface. In the bottom trace, the direct and surface reflected functions overlap as a result of the reduction in bandwidth of the source signal. Clearly this situation does not allow a confident evaluation of the peak level associated with the direct path.

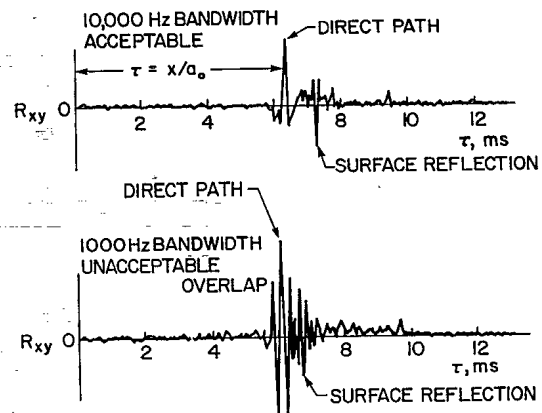


Figure 7. The Effect of Bandwidth on Correlation Function Overlap

A simple mathematical model of the cross-correlation function for the direct and surface reflected paths was developed by combining expressions for bandwidth-limited correlation functions given by Equation (11). Here  $\tau_1$  is the time for the sound to travel between the near and far-field sensors by the direct path and  $\tau_2$  the time for the reflected path. This model agreed well with results obtained using the J-11 projector driven with bandwidth-limited white noise, and so was used

$$R_{xy}(\tau) = a_1 B \left[ \frac{\sin B(\tau - \tau_1)}{\pi B(\tau - \tau_1)} \right] \cos 2\pi f_o(\tau - \tau_1) + a_2 B \left[ \frac{\sin \pi B(\tau - \tau_2)}{\pi B(\tau - \tau_2)} \right] \cos 2\pi f_o(\tau - \tau_2) \quad (11)$$

to develop criteria based on bandwidth and time delay for acceptable correlation functions.

A critical time delay ( $\Delta\tau_{crit}$ ) is defined as the time required for one of the correlation functions to decay to 10 percent of the peak value. Thus, when combining direct and surface reflected path correlation functions, this critical time delay represents a criterion which poses a maximum 10 per cent error on the peak value of the direct path correlation function. Using this criterion, a plot of the effect of source bandwidth and time delay on the correlation function overlap was generated, and is shown in Figure 8. This graph gives combinations of time delay difference,  $\Delta\tau$  (a function of the positioning of near and far-field sensors) and source bandwidth which will produce a correlation function with errors of less than 10 and 5 per cent. Clearly as the bandwidth of the source signal is reduced, the correlation function becomes more periodic and the required time delay difference becomes large. For a signal bandwidth of 1 kHz,  $\Delta\tau_{crit} = 2.50$  ms, which corresponds to a path length difference between the surface and reflected paths of 3.75 m.

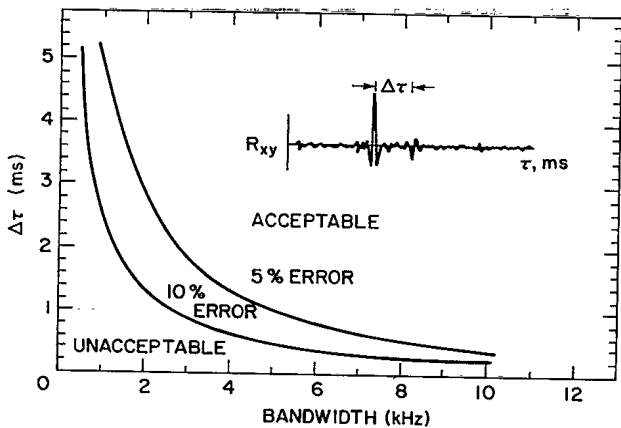


Figure 8. Criterion for Minimizing Correlation Function Overlap

The effective frequency range of the pressure gradient hydrophone designed for the cross-correlation experiments is in excess of 10 kHz. For these tests, the near-field pressure gradient hydrophone and far-field hydrophone were positioned to give a  $\Delta\tau$  of 4 ms, giving an expected overlap error of less than 1 percent.

### Propeller Wake Scans

Wake scans were carried out with the three experimental propellers to determine the location of noise sources along the propeller axis. To perform this experiment, the length of the hydrophone nose was reduced from 85 mm to 34 mm so that the pressure difference pair of elements could be positioned as close as possible to the propeller blade tips. The hydrophone was positioned 25 mm from the blade tip as shown in Figure 9, and moved axially, starting upstream of the propeller, in 50 mm steps from nominally 350 mm upstream to 1500 mm downstream. This distance spanned the propeller, wake development, and cavitation collapse sectors of the cylindrical control volume around the propeller and its wake.

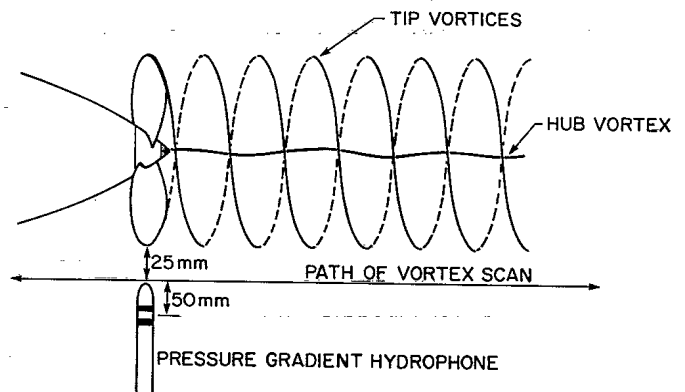


Figure 9. Arrangement for Wake Axial Traverse

At each measurement point, the pressure gradient and far-field signals were measured, amplified, filtered between 1 and 18 kHz, and recorded for later analysis. A portable correlation computer and spectrum analyser were available to verify data as they were being recorded.

Two wake scans were carried out with the Back Bubble propeller while only one was done with each tip vortex propeller. The cavitation states for the propellers were observed and photographed through the periscope. Table 1 lists the conditions for each of the three propellers.

Table 1. Test Conditions

Propeller	rpm	Cavitation States
Tip Vortex No. 1	1667	Tip Vortex
Tip Vortex No. 2	1667	Tip Vortex Hub Vortex
Back Bubble	1667	Bubble Tip Vortex Hub Vortex
Back Bubble	1433	Tip Vortex Hub Vortex

All propellers were tested at 1667 rpm. The Back Bubble propeller was also tested at a lower rate to investigate the influence on pressure gradient and source strength distribution of the disappearance of bubble cavitation.

The recorded data were analysed using a Saicor correlation computer linked to a PDP 11/34 mini-computer. The results included averaged spectra of the near-field pressure gradient and the far-field noise, and the acoustic source strength at each discrete location along the cylindrical control volume surface where measurements were taken. These latter values were plotted as a function of the axial distance to give a source strength distribution.

## RESULTS

### Pressure Gradient and Acoustic Spectra

Typical spectra for the near-field pressure gradient and far-field sound power for each propeller are shown in Figures 10 and 11, respectively. The pressure-gradient spectra were measured at a point 254 mm downstream of the propeller plane with the propellers turning at a rate of 1667 rpm. The spectra are relatively flat between 1 and 18 kHz, except at 6 kHz where a dip of about 5 dB occurs consistently in all curves. This is an anomaly inherent in the measurement system. However, because it was consistent in all spectra, and because it occupied a relatively narrow band, it does not affect the end results.

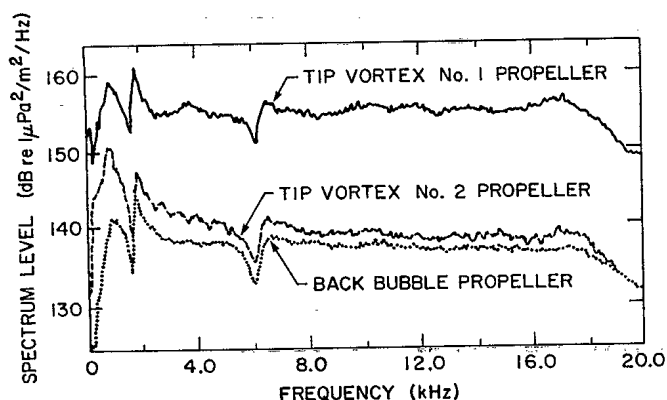


Figure 10. Pressure Gradient Spectra, 1667 rpm

The high pressure gradient amplitude associated with the Tip Vortex No. 1 propeller is consistent with the results from the far-field hydrophone (Figure 11). As can be seen from Figure 11, the level from this propeller exceeds those of the other two by as much as 19 dB. It also absorbed about 30 percent more power than the other two. This factor alone cannot explain the large difference between the level of its spectrum and those of the other two. Comparisons of spectrum levels at conditions of equal power

showed that the Tip Vortex No. 1 propeller was consistently noisier in the range of revolution rates from 1250 to 1800 rpm. The biasing of the loading toward the tip of this propeller would result in a stronger tip vortex, a greater amount of cavitation, and more noise.

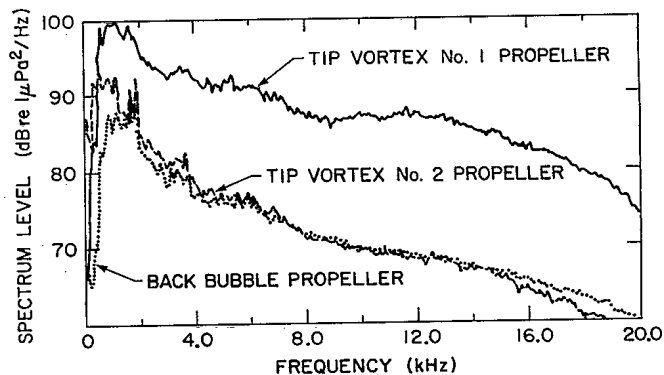


Figure 11. Far-Field Sound Spectra, 1667 rpm

### Near-Field Pressure Gradient

In the near-field of the propeller, the pressure gradient receives contributions from both hydrodynamic and acoustic pressure fluctuations. Generally, the hydrodynamic pressures are dominant, but do not propagate acoustically. Thus, the pressure gradient measurements alone will not necessarily reveal the true distribution of acoustic source strength in the propeller near-field. However, when used together, the pressure gradient and acoustic source strength information provide a powerful means of investigating cavitation noise generation.

The variation of near-field pressure gradient with axial distance along the propeller wake for the Tip Vortex No. 1, Tip Vortex No. 2, and Back Bubble propellers are shown in Figures 12, 13 and 14. The distances are referenced to the plane of the propeller. Negative numbers indicate distances upstream of the propeller plane, and positive numbers downstream.

The pressure gradient curve for the Tip Vortex No. 1 propeller rises to a broad peak 250 mm downstream of the propeller. The rise to and decay from this peak are rapid, indicative of a localized region of significant pressure gradient. Observations of the development of the cavitation revealed that this region of high pressure gradient occurred at the point where the tip vortex cavitation collapsed.

The near-field pressure gradient for the Tip Vortex No. 2 propeller are shown in Figure 13. As shown in Table 1, the curve corresponds to a condition with both tip and hub vortex cavitation on the propeller. The curve shows a rise in the pressure gradient at the point downstream where the cavitating vortices were observed to collapse. The curve decays rapidly with increasing axial distance beyond the region of vortex collapse.

Taken collectively, these curves suggest that the regions of high pressure gradient are associated with the collapse of cavitation voids. These regions appear to be relatively localized considering the resolution capabilities of the pressure gradient hydrophone. The pressure gradient rises and decays quickly outside the region of high pressure gradient.

Acoustic Source Strength

The results of the cross-correlation between the near-field pressure gradient and the far-field acoustic pressure were employed with Equation (10) to derive values for the acoustic source strength at a number of points in the near-field of the propeller. The results of the calculations are shown in Figures 15, 16 and 17, for the Tip Vortex No. 1 propeller, Tip Vortex No. 2 propeller, and Back Bubble propeller, respectively.

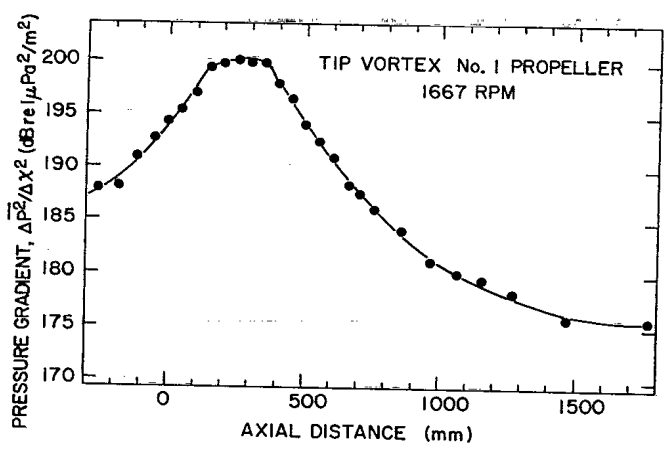


Figure 12. Pressure Gradient, Tip Vortex No. 1 Propeller

The difference in the pressure gradient curves for the Back Bubble propeller with and without bubble cavitation are shown in Figure 14. The top curve, which has two distinct peaks, corresponds to the condition with bubble, and tip and hub vortex cavitation present on the blades. The first peak occurs adjacent to the plane of the propeller and is probably associated with the bubble cavitation collapse on the back of the blades. The pressure gradient associated with the back bubble cavitation is greater than that for the vortex cavitation. The second peak, 350 mm downstream of the propeller plane, is produced by the collapse of the cavitation in the tip and hub vortices. The lower curve, which shows the results from a condition with no bubble cavitation present, has only one peak which is associated with the collapse of the tip and hub vortex cavitation.

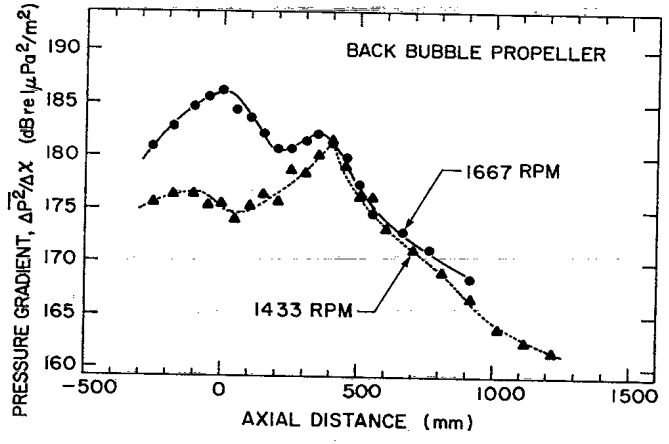


Figure 14. Pressure Gradient, Back Bubble Propeller

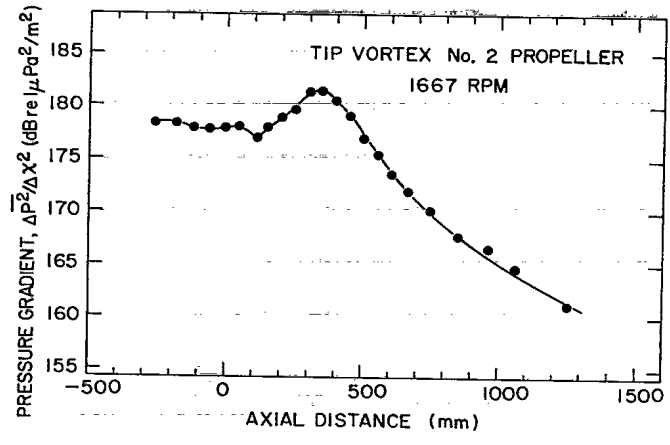


Figure 13. Pressure Gradient, Tip Vortex No. 2 Propeller

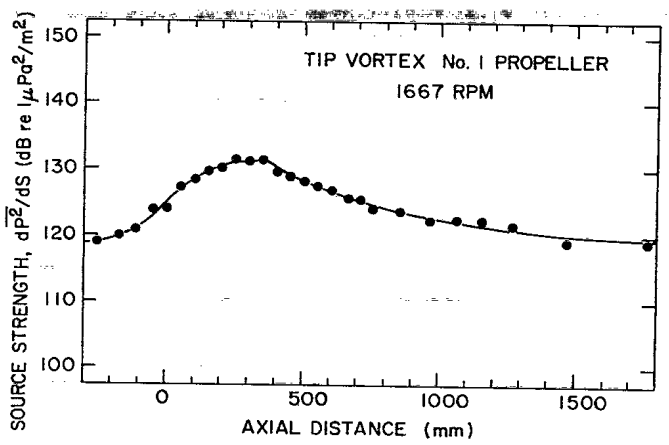


Figure 15. Source Strength Distribution, Tip Vortex No. 1 Propeller

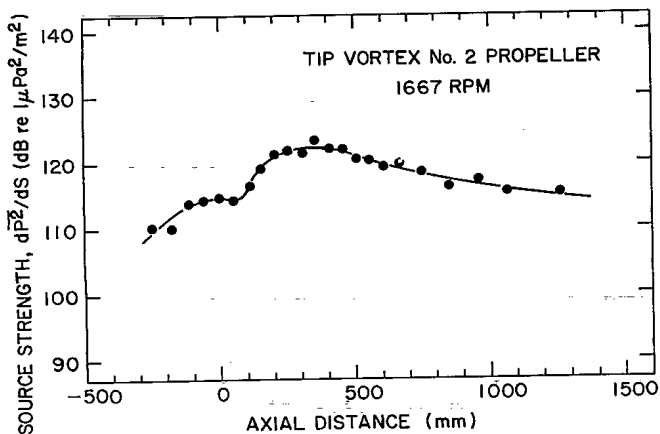


Figure 16. Source Strength Distribution, Tip Vortex No. 2 Propeller

The acoustic source strength distribution for the Tip Vortex No. 1 propeller (Figure 15) shows that the majority of sound from this propeller condition is originating downstream of the propeller in the region of vortex collapse. The source strength 350 mm downstream is 8 dB higher than that at the propeller plane. By comparing Figure 15 with Figure 12, it is apparent that the rate of decay with distance of the pressure gradient is very much more rapid than that of the acoustic source strength. For axial distances between 500 and 1000 mm, the level of pressure gradient reduces by 13 dB, while the acoustic source strength only falls by 6 dB. This result suggests that acoustic sources are present in the wake far downstream of the point of vortex collapse. This could be explained by the rebounds of small bubbles, produced when the vortices collapse. These sources which would convect downstream in the wake of the propeller, would not contribute greatly to the pressure gradient in the near-field, but would radiate acoustically.

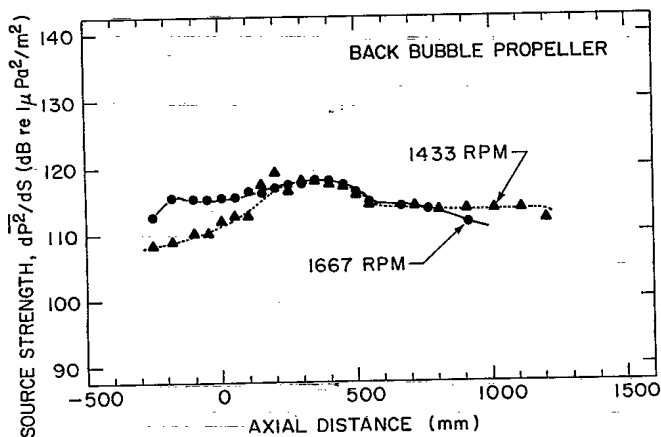


Figure 17. Source Strength Distribution, Back Bubble Propeller

The results for Tip Vortex No. 2 propeller, shown in Figure 16, show that the majority of noise in the far-field originates from the point of vortex cavitation collapse about 350 mm downstream of the propeller, as for the Tip Vortex No. 1 propeller. However, for this propeller, where the vortex is less intense, the source strength is some 7 dB less. This Figure also shows a slow rate of decay of the acoustic source strength with axial distance.

The acoustic source strength distributions for the Back Bubble propeller are shown in Figure 17 and should be compared with the pressure gradient curves of Figure 14. The main difference between the two sets of curves is that the change in acoustic source strength at the propeller plane location when the bubble cavitation disappears is small relative to the change in pressure gradient. The difference in acoustic source strength is 4 dB as opposed to 12 dB for the pressure gradient. Further, the acoustic source strength of the bubble cavitation is slightly less than that for vortex cavitation collapse. This result also seems to be at variance with the pressure gradient data. However, hydrodynamic and acoustic pressure fluctuations contribute to the pressure gradient. The results suggest that the bubble cavitation produces high hydrodynamic pressure gradient levels, which do not propagate acoustically, and that the source strength of the tip vortex and bubble cavitation are of the same order for this condition. The slow rate of decay of the source strength curve with axial distance could result from bubble rebounds in the wake as was the case for the other two propellers.

#### Source Strength Integration

If the distribution of acoustic source strength is integrated over the cylindrical surface with a radius equal to the radial position of the pressure gradient hydrophone, and length equal to the axial distance surveyed, the result should be equal to the overall sound level measured at the far-field hydrophone (see Equation (10)). Table 2 shows a comparison of values of  $\overline{p^2}$ , measured in the far-field, and those calculated by integrating the curves of Figures 15, 16, and 17 over the cylindrical surface.

Propeller	rpm	$\overline{p^2}$ Far Field dB	$\overline{p^2}$ Integrated dB
Tip Vortex	1667	135.0	131.0
Tip Vortex	1667	123.0	121.9
Back Bubble	1667	121.0	117.6
Back Bubble	1433	120.0	117.7

All of the measured values exceed those calculated from the source strength data by 2

to 4 dB.

Some error results because the acoustic waves in the propeller near-field are non-planar. The pressure gradient hydrophone, which was calibrated by placing it in the far-field of a controlled source, has a sensitivity which is based on plane waves propagating over its two ceramic elements. When placed in a spherical wave field the sensitivity of the pressure gradient hydrophone must be decreased in accordance with the correction factor given in Reference 10. For purely spherical waves, this correction would lead to an increase in the source strength of 4 dB. However, in the case of these wake scans, where the source may not be an ideal point source the factor is not easily calculated, but can be expected to lie somewhere between 0 and 4 dB. Work is presently underway to determine this correction for a distributed source.

Some error may also result if the entire noise producing region of the wake was not surveyed, as could have been the case in Figure 17.

If the measured value of  $\overline{p^2}$  in the far-field is identical to that calculated by integrating the source strength distribution, all sound is being produced by the mechanism related to the pressure gradient fluctuations which are generated by the normal acceleration of the cavitation voids. Complete agreement would thus indicate that the acoustic source mechanisms of vortex and bubble cavitation are monopole in nature, and higher order mechanisms would be insignificant.

#### CONCLUDING REMARKS

This paper has described a method for determining the distribution of acoustic source strength in the near-field of a cavitating propeller by the use of cross-correlation. The technique described offers a powerful method for finding the mechanisms and locations of sound generation on and near the propeller.

Results indicate that for propellers producing vortex types of cavitation, the noise is produced by the collapse of the cavitating vortices at points downstream of the propeller plane. Bubble rebounds following the point of collapse are suspected of being responsible for the slow decay of the sound-producing regions in the propeller wake with distance downstream.

Propellers which develop both bubble and vortex types of cavitation produce an acoustic source strength distribution which is nearly constant from the propeller plane to the point of vortex cavitation collapse. Such a result could be explained by bubbles produced at the blade rebounding near the propeller, and by the tip and hub vortices collapsing farther downstream. The bubble cavitation produces high levels of pressure gradient compared to the pressure gradients associated with the vortex collapse region. However, as the acoustic source strength of the two regions

are of the same order, the strong pressure gradient field of the bubble cavitation is relatively inefficient acoustically compared to the region of the vortex collapse.

#### REFERENCES

1. Curle, N., "The Influence of Solid Boundaries on Aerodynamic Sound," Proc. Roy. Soc. (London), Ser. A231, 1955 pp. 505-514.
2. Siddon, T.E., "Surface Dipole Strength by Cross-Correlation Method," JASA., Vol. 53, No. 2, Feb. 1973, pp. 619-633.
3. Leggat, L.J., Siddon, T.E., "Experimental Investigations of the Aeroacoustic Mechanism of Rotor-Vortex Interactions," JASA., Vol. 64, No. 4, Oct. 1978, pp. 1070-1077.
4. Regan, D.R. Meecham, W.C., "Multiple Turbojet Noise-Suppression Studies Using Cross-Correlation Techniques," JASA., Vol. 63, No. 6, June 1978, pp. 1753-1767.
5. Pan, Y.S., "Cross-Correlation Methods for Studying Near and Far-Field Noise Characteristics of Several Flow-Surface Interaction Problems," Presented to the 87th meeting of the ASA, Apr. 1974.
6. Lighthill, M.J., "Sound Generated Aerodynamically," Proc. Roy. Soc., A267, 1962, pp. 147-182.
7. Leggat, L.J., "Propeller Cavitation Noise Investigations in a Free-Field Environment," Presented to the DRG Seminar on Advanced Hydrodynamic Testing Facilities, The Hague, Apr. 1982.
8. McMahon, G.W., "New Floating Laboratory Facilities Underwater Acoustic Measurement," Canadian Electronics Engineering, Feb. 1961.
9. Fanning, B.L., "A Pressure Gradient Hydrophone for Propeller Noise Studies," DREA Informal Communication, Oct. 1981.
10. Bobber, R.J., Underwater Electroacoustic Measurement, Naval Research Laboratory, Washington, D.C., July 1970.

reprinted from

**International Symposium on Cavitation Noise**

Editors: R. E. A. Arndt and M. L. Billet

(Book No. H00231)

published by

**THE AMERICAN SOCIETY OF MECHANICAL ENGINEERS**

345 East 47th Street, New York, N.Y. 10017

Printed in U.S.A.



DOCUMENT CONTROL DATA - R & D		
(Security classification of title, body of abstract and indexing annotation must be entered when the overall document is classified)		
1. ORIGINATING ACTIVITY Defence Research Establishment Atlantic	2a. DOCUMENT SECURITY CLASSIFICATION Unclassified	
	2b. GROUP	
3. DOCUMENT TITLE The Study of Propeller Cavitation Noise Using Cross-Correlation Methods		
4. DESCRIPTIVE NOTES (Type of report and inclusive dates) DREA Report		
5. AUTHOR(S) (Last name, first name, middle initial) Leggat, L. John, Sponagle, Neil C.		
6. DOCUMENT DATE December 82	7a. TOTAL NO. OF PAGES 16	7b. NO. OF REFS 10
8a. PROJECT OR GRANT NO.	9a. ORIGINATOR'S DOCUMENT NUMBER(S) DREA Report 82/5	
8b. CONTRACT NO.	9b. OTHER DOCUMENT NO.(S) (Any other numbers that may be assigned this document)	
10. DISTRIBUTION STATEMENT Unlimited		
11. SUPPLEMENTARY NOTES	12. SPONSORING ACTIVITY DREA	
13. ABSTRACT  <p>This paper presents a technique for the study of the mechanisms responsible for the generation of noise from cavitating propellers. The experimental method, which involves the cross-correlation of the pressure gradient in the near-field of the propeller with far-field sound, allows the determination of the spatial distribution of acoustic source strength on and near the cavitating propeller.</p> <p>The paper describes the mathematical basis for the cross-correlation technique, and then presents some of the results from experiments with propellers specifically designed to produce vortex and bubble forms of cavitation.</p> <p>Cross-Correlations performed at a number of points along a track parallel to the axis of the propeller indicate that the majority of noise from propellers producing vortex cavitation originates from the region of vortex collapse. A bubble cavitation propeller showed a region of relatively constant source strength distribution from the propeller disk region downstream to the point of vortex collapse. All propellers tested showed a slow decay of acoustic source strength with downstream distance after vortex collapse. This result may be indicative of significant amounts of sound being produced by bubble rebounds in the propeller wake.</p>		

## KEY WORDS

Propeller Noise  
Cavitation  
Cross-Correlation  
Pressure-gradient  
Noise diagnostics

83-00646  
# 38697

## INSTRUCTIONS

1. **ORIGINATING ACTIVITY:** Enter the name and address of the organization issuing the document.
- 2a. **DOCUMENT SECURITY CLASSIFICATION:** Enter the overall security classification of the document including special warning terms whenever applicable.
- 2b. **GROUP:** Enter security reclassification group number. The three groups are defined in Appendix 'M' of the DRB Security Regulations.
3. **DOCUMENT TITLE:** Enter the complete document title in all capital letters. Titles in all cases should be unclassified. If a sufficiently descriptive title cannot be selected without classification, show title classification with the usual one-capital-letter abbreviation in parentheses immediately following the title.
4. **DESCRIPTIVE NOTES:** Enter the category of document, e.g. technical report, technical note or technical letter. If appropriate, enter the type of document, e.g. interim, progress, summary, annual or final. Give the inclusive dates when a specific reporting period is covered.
5. **AUTHOR(S):** Enter the name(s) of author(s) as shown on or in the document. Enter last name, first name, middle initial. If military, show rank. The name of the principal author is an absolute minimum requirement.
6. **DOCUMENT DATE:** Enter the date (month, year) of Establishment approval for publication of the document.
- 7a. **TOTAL NUMBER OF PAGES:** The total page count should follow normal pagination procedures, i.e., enter the number of pages containing information.
- 7b. **NUMBER OF REFERENCES:** Enter the total number of references cited in the document.
- 8a. **PROJECT OR GRANT NUMBER:** If appropriate, enter the applicable research and development project or grant number under which the document was written.
- 8b. **CONTRACT NUMBER:** If appropriate, enter the applicable number under which the document was written.
- 9a. **ORIGINATOR'S DOCUMENT NUMBER(S):** Enter the official document number by which the document will be identified and controlled by the originating activity. This number must be unique to this document.
- 9b. **OTHER DOCUMENT NUMBER(S):** If the document has been assigned any other document numbers (either by the originator or by the sponsor), also enter this number(s).
10. **DISTRIBUTION STATEMENT:** Enter any limitations on further dissemination of the document, other than those imposed by security classification, using standard statements such as:
  - (1) "Qualified requesters may obtain copies of this document from their defence documentation center."
  - (2) "Announcement and dissemination of this document is not authorized without prior approval from originating activity."
11. **SUPPLEMENTARY NOTES:** Use for additional explanatory notes.
12. **SPONSORING ACTIVITY:** Enter the name of the departmental project office or laboratory sponsoring the research and development. Include address.
13. **ABSTRACT:** Enter an abstract giving a brief and factual summary of the document, even though it may also appear elsewhere in the body of the document itself. It is highly desirable that the abstract of classified documents be unclassified. Each paragraph of the abstract shall end with an indication of the security classification of the information in the paragraph (unless the document itself is unclassified) represented as (TS), (S), (C), (R), or (U).  
The length of the abstract should be limited to 20 single-spaced standard typewritten lines; 7 1/4 inches long.
14. **KEY WORDS:** Key words are technically meaningful terms or short phrases that characterize a document and could be helpful in cataloging the document. Key words should be selected so that no security classification is required. Identifiers, such as equipment model designation, trade name, military project code name, geographic location, may be used as key words but will be followed by an indication of technical context.